JPE 15-5-14

http://dx.doi.org/10.6113/JPE.2015.15.5.1274
ISSN(Print): 1598-2092 / ISSN(Online): 2093-4718

MRAS Based Speed Estimator for Sensorless Vector Control of a Linear Induction Motor with Improved Adaptation Mechanisms

Mohammad Hosein Holakooie[†], Asghar Taheri[*], and Mohammad Bagher Bannae Sharifian[**]

[†,**]Department of Electrical and Computer Engineering, University of Tabriz, Tabriz, Iran
[*]Department of Electrical Engineering, University of Zanjan, Zanjan, Iran

Abstract

This paper deals with model reference adaptive system (MRAS) speed estimators based on a secondary flux for linear induction motors (LIMs). The operation of these estimators significantly depends on an adaptation mechanism. Fixed-gain PI controller is the most common adaptation mechanism that may fail to estimate the speed correctly in different conditions, such as variation in machine parameters and noisy environment. Two adaptation mechanisms are proposed to improve LIM drive system performance, particularly at very low speed. The first adaptation mechanism is based on fuzzy theory, and the second is obtained from an LIM mechanical model. Compared with a conventional PI controller, the proposed adaptation mechanisms have low sensitivity to both variations of machine parameters and noise. The optimum parameters of adaptation mechanisms are tuned using an offline method through chaotic optimization algorithm (COA) because no design criterion is given to provide these values. The efficiency of MRAS speed estimator is validated by both numerical simulation and real-time hardware-in-the-loop (HIL) implementations. Results indicate that the proposed adaptation mechanisms improve performance of MRAS speed estimator.

Key words: Adaptation mechanism, Fuzzy controller, Linear induction motor (LIM), Mechanical model, Model reference adaptive system (MRAS), Vector control.

I. INTRODUCTION

Recently, LIM has been widely used in industrial applications such as transportation systems. Compared with conventional structures (i.e., rotary electric motor and gear box), these types of motors remove all mechanical interfaces to produce a direct linear motion. The counterpart of this advantage is an asymmetric structure of LIM both in longitudinal and transversal directions, which creates the so-called longitudinal end effect and transversal edge effect, respectively. These phenomena increase the complexity of the LIM model and proper control of electromechanical characteristics of the LIM, such as thrust, magnetic flux, and linear speed.

Manuscript received Dec. 8, 2014; accepted May 11, 2015
Recommended for publication by Associate Editor Gaolin Wang.
[†]Corresponding Author: hosein.holakooie@gmail.com
Tel: +98-411- 3393715, Fax: +98- 411-3300829, Tabriz University
[*]Dept. of Electrical Engineering, University of Zanjan, Iran
[**]Dept. of Electrical and Computer Eng., University of Tabriz, Iran

LIM equivalent circuit (EC) has been vastly developed in technical literatures [1]-[8]. To address the mentioned subject, Nondal, et al. [1] and Wei xu, et al. [2] obtained an EC using a winding function theory for high speed double side LIM and single side LIM, respectively. Pai, et al. [3] derived an EC of LIM based on a field theory where longitudinal end effects, transversal edge effect, field diffusion in the secondary sheet, and back-iron saturation have been considered. Moreover, some researchers utilize one-dimensional (1-D) and two-dimensional (2-D) field theories to obtain EC of the LIM [4]-[6]. However, majority of these ECs describe the steady-state behavior of LIM. Huang, et al. [7] considered longitudinal end effect as a braking force in the mechanical equation of LIM. Duncan's EC [8] is similar to a rotary induction motor except that some modifications are applied to the parallel magnetizing branch to consider longitudinal end effect. This EC can describe both dynamic and steady-state behaviors of LIM.

Using the aforementioned ECs, various control

strategieshave been developed, in particular, direct/indirect vector controls [9]-[13]. Some of these strategies are based on mechanical sensors to provide linear speed [9]-[11] and the other one estimate speed using terminal voltage and current of LIM [12], [13]. Sung, et al. [9] employ a per-phase steady-state Duncan's EC to derive a dynamic model of LIM where Duncan's modifications are only executed in d-axis EC, whereas Kang, et al. [10] applied the modifications both in d-axis and q-axis ECs. Afterward, these papers presented an indirect vector control scheme based on a dynamic EC of LIM. Direct vector control scheme is developed in [11]; in this scheme, the "voltage model" and "current model" were deduced based on the space-vector equation of LIM. Then, a secondary flux angle is estimated by the flux models. In the case of vector control of LIM (with the speed loop), speed and position are measured by a linear encoder which is more expensive and less reliable versus a rotary machine. Hence, presenting a high-performance sensorless vector control of LIM is very challenging work; given the complexity of the machine model, very few studies have been proposed using this approach [12]. In particular, Cirrincione, et al. [12] have developed a neural network MRAS speed estimator for LIM based on Duncan's EC where several experiment results have been presented. Liu, et al. [13] considers the end effect as a braking force approximated by a third-order Taylor's series. Afterward, a fuzzy observer is presented to estimate linear speed and secondary flux.

In this paper, the main focus is on the MRAS speed estimator. Two adaptation mechanisms are proposed instead of a conventional PI controller, which would improve speed estimation, particularly at low speed. An indirect vector control method, described in [10], is used to properly control magnetic flux and linear speed. Optimum parameters of the proposed adaptation mechanisms are determined by an offline method through COA. First, a dynamic model of LIM is provided based on a steady-state Duncan's EC. Afterward, the details of the MRAS speed estimator with improved adaptation mechanisms are developed. Simulation and real-time HIL results are presented to demonstrate better performance of the proposed schemes against a conventional PI controller.

II. DYNAMIC MODEL OF LIM

The structure of LIM is shown in Fig. 1. In the LIM, during the primary (stator) movement, the secondary (rotor) is continuously replaced by a new material. Because of the appearance of this new material, the air-gap flux density gradually (not suddenly) increased at the entry of primary with total secondary time constant described in: $T_r = (L_m + L_{lr}) / R_r$, where L_m , L_{lr} , and R_r are magnetizing inductance, secondary leakage inductance and secondary resistance, respectively. The flux density decreased

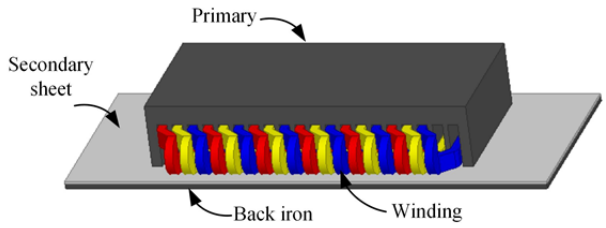

Fig. 1. Structure of LIM.

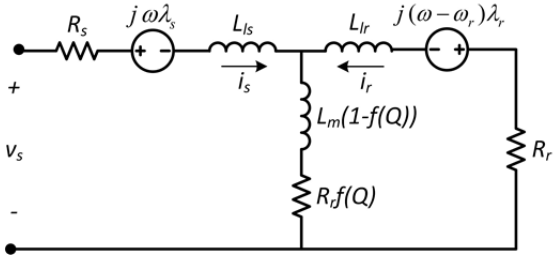

Fig. 2. Space vector equivalent circuit of LIM.

at the exit of primary with secondary leakage time constant show in: $T_r' = L_{lr} / R_r$. Increasing and decreasing the air-gap flux density cause an eddy current in the secondary sheet. The eddy current deteriorates the air-gap flux density in longitudinal direction as well as increases ohmic losses. Such phenomenon is called end effect. Duncan described this effect by end effect factor [8]:

$$Q = \frac{T_v}{T_r} = \frac{L_p / v_l}{(L_m + L_{lr}) / R_r} \tag{1}$$

The term $T_v = L_p / v_l$ is the time of traverse of an imaginary point by the primary core where L_p and v_l are the primary length and linear speed, respectively. The magnetizing inductance is modified by this factor which is shown below:

$$M = L_m (1 - f(Q)) \tag{2}$$

where:

$$f(Q) = \frac{1 - e^{-Q}}{Q} \tag{3}$$

The space vector EC of LIM is shown in Fig. 2. The term $R_r f(Q)$ demonstrates the ohmic losses due to end effect. EC is similar to rotary induction motor except that some modifications are applied to a parallel magnetizing branch. The voltage equations in arbitrary reference frame are as follows:

$$v_s = R_s i_s + j\omega\lambda_s + p\lambda_s + R_{sh}(i_s + i_r) \tag{4}$$

$$v_r = 0 = R_r i_r + j(\omega - \omega_r)\lambda_r + p\lambda_r + R_{sh}(i_s + i_r) \tag{5}$$

The flux linkage equations are as follows:

$$\lambda_s = L_s i_s + M i_r \tag{6}$$

$$\lambda_r = L_r i_r + M i_s \tag{7}$$

with:

$$L_s = L_{ls} + M \tag{8}$$

$$L_r = L_{lr} + M \tag{9}$$

$$R_{sh} = R_r f(Q) \tag{10}$$

where R_s and R_r are the primary and secondary resistances, i_s and i_r are the primary and secondary currents, λ_s and λ_r are the primary and secondary flux linkages, L_s and L_r are the primary and secondary self inductances, ω_r is angular electrical speed of primary, and j is the imaginary unit. The electromagnetic thrust generated by LIM is calculated as follows:

$$F_e = \frac{3}{2}\frac{p}{2}\frac{\pi}{\tau}\mathrm{Re}(j\lambda_s i_s) \tag{11}$$

where p and τ are the pole number and the pole pitch, respectively.

III. Flux Estimator Based on Machine Model

The amplitude and angle of flux linkage are two important variables that need to be estimated in direct/indirect vector control schemes. Flux estimators are generally obtained from voltage equations in the same reference frame. Therefore, one of the flux estimators always depends on linear speed. Employing flux models in an adaptive scheme establishes MRAS speed estimator. The so-called voltage model and current model are derived from primary and secondary voltage equations, respectively, as flux estimators.

Some assumptions are applied to dynamic equations of LIM [3], [11]:

- The secondary leakage inductance is zero. ($L_{lr} = 0$)
- The rate of change of linear speed is zero. ($\frac{dv_l}{dt} = 0$)

Using equation (4) in stationary reference frame ($\omega = 0$) and equations (6) and (7) with some mathematical manipulation, the voltage model is derived as follows:

$$p\lambda_r = v_s - R_s i_s - pL_{ls} i_s - \frac{R_{sh}}{M}\lambda_r \tag{12}$$

Using equation (5) in primary reference frame ($\omega = \omega_r$) and equations (6) and (7), the current model is obtained as follows:

$$p\hat{\lambda}_r = R_r i_s - \frac{R_r + R_{sh}}{M}\hat{\lambda}_r + j\omega_r\hat{\lambda}_r \tag{13}$$

Given that $\omega_r = \frac{P}{2}\frac{\pi}{\tau}v_l$, if equations (12) and (13) are decomposed in their real and imaginary parts, the following four scalar equations is provided:

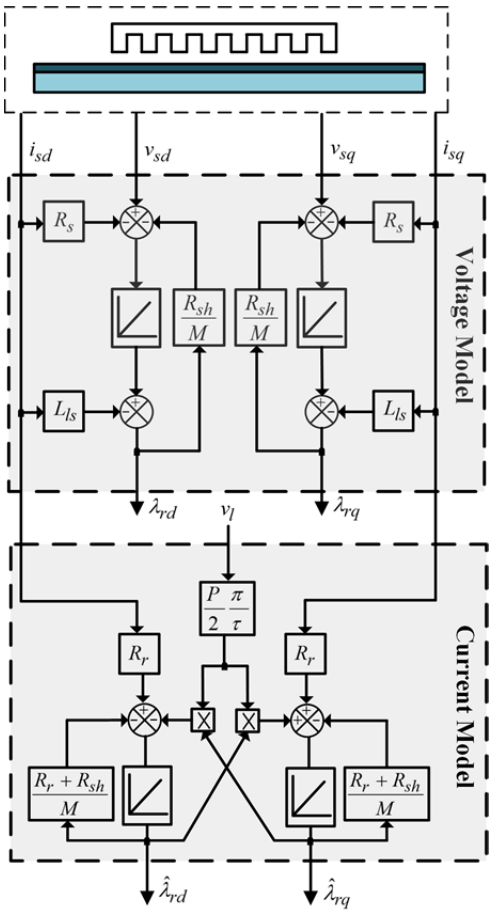

Fig. 3. The structure of voltage and current model.

$$\begin{cases} p\lambda_{rd} = v_{sd} - R_s i_{sd} - pL_{ls} i_{sd} - \dfrac{R_{sh}}{M}\lambda_{rd} \\ p\lambda_{rq} = v_{sq} - R_s i_{sq} - pL_{ls} i_{sq} - \dfrac{R_{sh}}{M}\lambda_{rq} \\ p\hat{\lambda}_{rd} = R_r i_{sd} - \dfrac{R_r + R_{sh}}{M}\hat{\lambda}_{rd} - \dfrac{P}{2}\dfrac{\pi}{\tau}v_l\hat{\lambda}_{rq} \\ p\hat{\lambda}_{rq} = R_r i_{sq} - \dfrac{R_r + R_{sh}}{M}\hat{\lambda}_{rq} + \dfrac{P}{2}\dfrac{\pi}{\tau}v_l\hat{\lambda}_{rd} \end{cases} \tag{14}$$

The voltage model and the current model, described by Equation (14) are shown in Fig. 3. The current model needs linear speed to obtain secondary flux, whereas the voltage model decouples from the linear speed.

IV. MRAS Based Speed Estimator

Among the different schemes for sensorless control of induction machine, MRAS speed estimator is widely used because of its simple structure and low computation [14]. This estimator is constituted from two different models, namely reference model and adjustable model, but both estimates the same state variable. The voltage and current model, described in previous section, are considered as a

reference and adjustable model, respectively. In this paper, MRAS speed estimator is based on a secondary flux (i.e., the voltage and current model estimate the secondary flux).

In the MRAS speed estimator strategy, linear speed is operated as an adaptive parameter and continuously returned to the current model by an adaptation mechanism. The adaptation mechanism must be designed to ensure stability of the system. For this purpose, MRAS speed estimator generally can be represented by two basic subsystems, namely, linear time-invariant feedforward and nonlinear time-variant feedback subsystems. Then, the adaptation mechanism is designed according to Popov's hyperstability theory [15] and [16]. Starting from the current model and subtract it from the corresponding equations for the voltage model, the state-space error equations can be written as follows:

$$p\begin{bmatrix}\varepsilon_d\\ \varepsilon_q\end{bmatrix}=\begin{bmatrix}-\dfrac{R_r+R_{sh}}{M} & -\dfrac{p}{2}\dfrac{\pi}{\tau}v_l\\ \dfrac{p}{2}\dfrac{\pi}{\tau}v_l & -\dfrac{R_r+R_{sh}}{M}\end{bmatrix}\begin{bmatrix}\varepsilon_d\\ \varepsilon_q\end{bmatrix}+\frac{p}{2}\frac{\pi}{\tau}\begin{bmatrix}-\hat{\lambda}_{rq}\\ \hat{\lambda}_{rd}\end{bmatrix}(\hat{v}_l-v_l) \tag{15}$$

where $\varepsilon_d=\hat{\lambda}_{rd}-\lambda_{rd}$ and $\varepsilon_q=\hat{\lambda}_{rq}-\lambda_{rq}$ denote secondary flux errors in d-axis and q-axis, respectively. This equation can be written as

$$p\boldsymbol{\varepsilon}=\mathbf{A}\boldsymbol{\varepsilon}-\mathbf{W} \tag{16}$$

where $\mathbf{A}$ is the state matrix.

According to Popov's criterion for stability, the linear time-invariant feedforward transfer matrix must be strictly positive real. In this study, the feedforward transfer matrix is $\mathbf{F}(s)=[s\mathbf{I}-\mathbf{A}]^{-1}$, where $\mathbf{I}$ is the identity matrix. With extensive calculation, this matrix is positive and real. On the other hand, nonlinear time-variant feedback subsystem must fulfill Popov's integral inequality as follows:

$$\int_0^{t1}\boldsymbol{\varepsilon}^T\mathbf{W}dt\geq 0 \tag{17}$$

If Popov's inequality is solved in time interval $[0\quad t_1]$ for all $t_1\geq 0$, then a proper candidate adaptation mechanism is expressed as $\hat{v}_l=F_p(\varepsilon)+\int F_i(\varepsilon)d_\tau$ and substitute the error matrix from equation (15) in (17), then the adaptation mechanism is derived as

$$F_p=K_p\varepsilon_v \tag{18}$$

$$F_i=K_i\varepsilon_v \tag{19}$$

where ε_v is speed tuning signal defined as follows:

$$\varepsilon_v=\lambda_{rq}\hat{\lambda}_{rd}-\lambda_{rd}\hat{\lambda}_{rq} \tag{20}$$

The structure of MRAS speed estimator is shown in Fig. 4. The speed tuning signal is an important parameter in MRAS

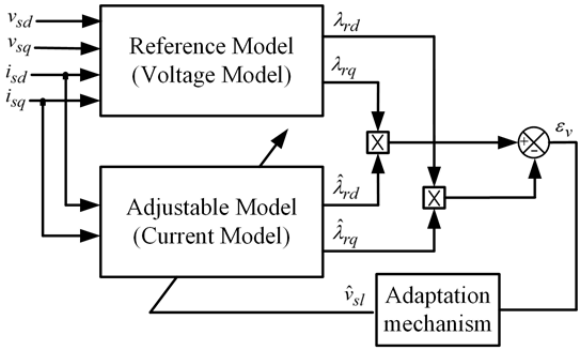

Fig. 4. MRAS based speed estimator.

speed estimator which is acquired by Popov's hyperstability theory with PI controller as an adaptation mechanism candidate. This parameter is successfully applied to two other adaptation mechanisms (described in the next sections) and stability of the system is observed for a wide range of linear speed from low speed to twice rated speed with rated load force.

In MRAS speed estimator, linear speed is used as an adaptive variable. The adaptation mechanism obtains the linear speed from the speed tuning signal. Therefore, the quality of estimated speed is related to the operation of adaptation mechanism. PI controllers are generally used in industrial applications because of its simple structure. This controller can properly estimate linear speed over a wide speed range. However, several factors, such as variation of machine parameters, nonlinear properties of voltage source inverter and measurement noise, affect the operation of PI controller, especially at low speed [14]. In the next sections, two robust adaptation mechanisms replace the PI controller.

V. ADAPTATION MECHANISM BASED ON FUZZY CONTROLLER

A fuzzy logic is an interesting method to formulate human knowledge. This method is based on fuzzy rules, which can be obtained through the knowledge of experts. Among various applications of fuzzy logic method, fuzzy controller is important in literature. The fuzzy controller is very suitable for control, estimation and optimization of complex nonlinear dynamic systems, such as induction machines [15].

In this paper, a fuzzy controller is used as a robust adaptation mechanism to estimate linear speed. The structure of fuzzy controller is shown in Fig. 5. The inputs of this controller are speed tuning signal and its changes, and the output is an estimated linear speed of LIM. This controller consists of three basic parts: fuzzification process, inference engine based on fuzzy rules (a set of If-Then rules), and defuzzification process. Each definitive input point is mapped to a fuzzy set by fuzzifier and the reverse process is done by a defuzzifier. The inference engine obtains an output fuzzy set

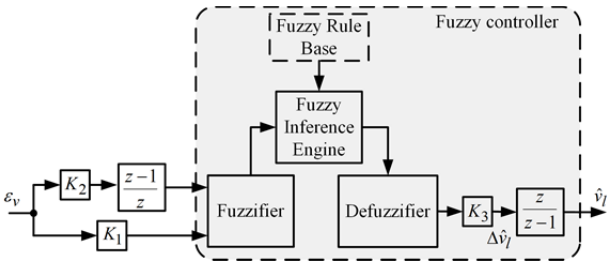

Fig. 5. Fuzzy controller.

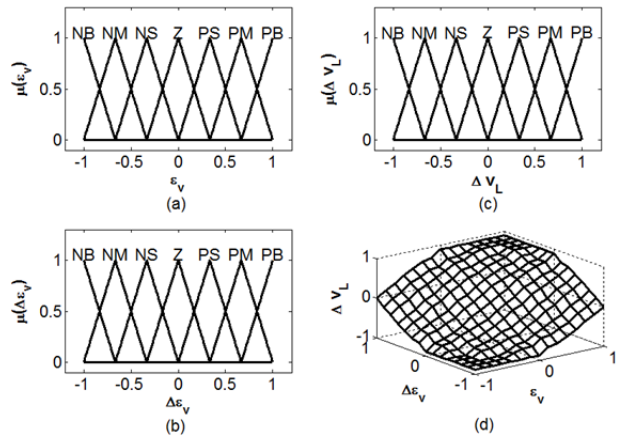

Fig. 6. Membership functions of (a) speed tuning signal (b) changes of speed tuning signal (c) changes of estimated linear speed and (d) nonlinear surface of inputs/output.

using a rule base generated from human knowledge. In this study, the center average (CA) method is used as defuzzifier which can be expressed as follows:

$$X = \frac{\sum_{i=1}^{N} X_i \ \mu(X_i)}{\sum_{i=1}^{N} \mu(X_i)} \tag{21}$$

where N is the number of rules, $\mu(X_i)$ is the membership grade of the fuzzy output X_i given by i th rule.

Appropriate determination of fuzzy rules is the most important step for design of fuzzy controller because of the direct impact of the rules on the dynamic and steady-state errors of the system. One common method for selection of rules in adaptive scheme applications is the symmetric approach where the matrix of fuzzy rules has a symmetric distribution [17]. The fuzzy rules produced by this approach are shown in Table I.

The fuzzification and defuzzification processes are completed by means of symmetrical triangular membership functions which provide a desirable dynamic and steady-state performance. The membership functions of inputs and output are shown in Figs. 6(a), (b), and (c), respectively.

Also, Fig. 6(d) demonstrates nonlinear surface of inputs and output which is acquired by mapping the relationship between input and output variables according to a fuzzy rule base. Since the matrix of fuzzy rules has a symmetric distribution, the nonlinear surface of fuzzy controller continuously decreased.

TABLE I
MATRIX OF FUZZY RULES

$\Delta\varepsilon_v$ \ ε_v	NB	NM	NS	Z	PS	PM	PB
NB	NB	NB	NB	NB	NM	NS	Z
NM	NB	NB	NB	NM	NS	Z	PS
NS	NB	NB	NM	NS	Z	PS	PM
Z	NB	NM	NS	Z	PS	PM	PB
PS	NM	NS	Z	PS	PM	PB	PB
PM	NS	Z	PS	PM	PB	PB	PB
PB	Z	PS	PM	PB	PB	PB	PB

In the fuzzy controller, the output and each of the inputs are described by the following 7 membership functions: NB (Negative Big), NM (Negative Medium), NS (Negative Small), Z (Zero), PS (Positive Small), PM (Positive Medium), and PB (Positive Big). This matrix is created by 7×7 rules because the inputs are labeled by 7 membership functions. The membership functions are considered in normalized form.

To obtain the actual value of the rate of change of the estimated speed $\Delta\hat{v}_l$, the inputs are multiplied by two coefficients K_1 and K_2, the output is multiplied by coefficient K_3 and the estimated linear speed is calculated as

$$\hat{v}_l(k) = \hat{v}_l(k-1) + \Delta\hat{v}_l(k) \tag{22}$$

VI. ADAPTATION MECHANISM BASED ON MECHANICAL MODEL

To improve transient operation of MRAS speed estimator, the mechanical equation of LIM can be used in the adaptation mechanism [18]. These equations are as follows:

$$\dot{\hat{v}}_l = \frac{1}{m}(\hat{F}_e - \hat{F}_l) \tag{23}$$

$$\dot{\hat{F}}_l = 0 \tag{24}$$

Because of the simplicity of the mechanical equation, the load force is assumed as a constant value while the friction force is neglected. The speed tuning signal is added to the above equation as a proportional correction term:

$$\dot{\hat{v}}_l = \frac{1}{m}(\hat{F}_e - \hat{F}_l) + K_{pv}\varepsilon_v \tag{25}$$

$$\dot{\hat{F}}_l = K_{pf}\varepsilon_v \tag{26}$$

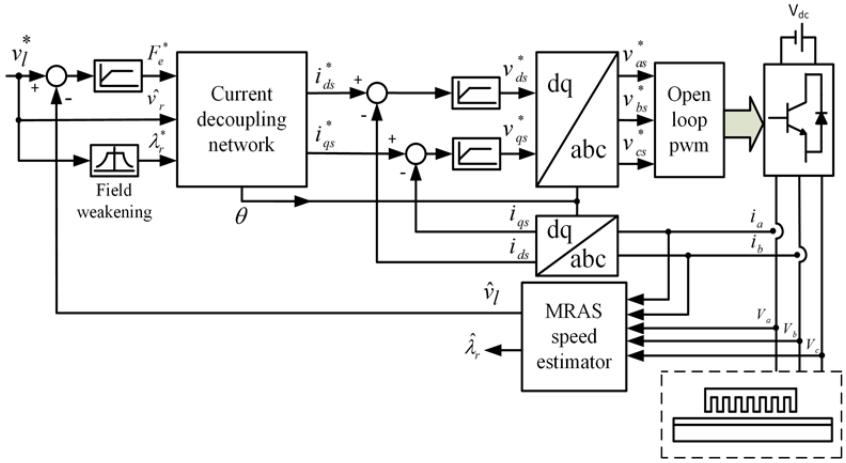

Fig. 7. Block diagram of sensorless indirect vector control.

where K_{pv} and K_{pf} are the speed and force gain, respectively. Using equations (25) and (26), both linear speed and load force can be estimated using the speed tuning signal. In this paper, the parameters of all studied adaptation mechanisms are provided by COA.

VII. CHAOTIC OPTIMIZATION ALGORITHM

Most problems, such as optimal design of fuzzy controller in the complex nonlinear system, can be developed as an optimization problem. Global optimum detection is one of the most important factors in optimization algorithms. Most heuristic optimization algorithms have been introduced in technical literatures such as genetic algorithm (GA), particle swarm optimization (PSO), simulated annealing (SA), and COA, which try to find a global optimal point. The main features of COA are as follows [19], [20]:

- Distinguishes between local and global optimal points by its inherent powerful structure,
- Does not produce repetitive numbers in searching progress,
- Easily implemented and running time is fairly short.

The COA usually has two main steps as follows [20]:

Step 1: Mapping a generated sequence of chaotic points from the chaotic space to the solution space and then providing a current optimum point with respect to the objective function.

Step 2: Obtaining a global optimal point using current optimal point and chaotic dynamics.

Accurate determination of adaptation mechanism parameters has a significant role in the level of quality of estimated speed. A trial-and-error method is conventionally adopted for such nonlinear problems. However, optimum coefficients of the controllers may not be obtained by this method. An optimization technique, such as COA, provides an intelligent trial-and-error process. As a result, the COA is adopted to determine adaptation mechanism coefficients. For this purpose, an objective function is defined as follows:

$$f = \int_0^{t_{sim}} t|\Delta v_l|dt \tag{27}$$

where Δv_l is the error of real and estimated speed and t_{sim} is the simulation time. The results of COA for adaptation mechanism parameters are shown in the Appendix.

VIII. SIMULATION RESULTS

The operation of MRAS speed estimator with the proposed adaptation mechanisms is verified using numerical simulation. For this purpose, the Matlab/Simulink software is adopted. The block diagram of the computer simulation model is shown in Fig. 7. According to this figure, linear speed is obtained using terminal voltages and currents of LIM. Afterward, the estimated speed is used in the current decoupling network to provide the command values of currents in the synchronous reference frame. The error of currents is applied to PI controller to provide voltage commands similarly in the synchronous reference frame. Some other details of the indirect vector control scheme are presented in [10]. In this study, a single sided LIM chooses which parameters of motor are shown in the Appendix.

A. Rated Speed Operation

The operation of indirect vector control strategy with MRAS speed estimator for PI, fuzzy, and mechanical adaptation mechanisms at rated speed is shown in Figs. 8(a), (b) and (c), respectively. In this case, the command value of linear speed is increased from $0.2\,m/s$ to $4\,m/s$ (from low speed to rated speed) as a step function at $t = 2s$. The command value of thrust is $30\,N$. The indirect vector control is based on a secondary flux orientation and the command value of secondary flux is $0.77\,Wb$. From this figure, the estimated

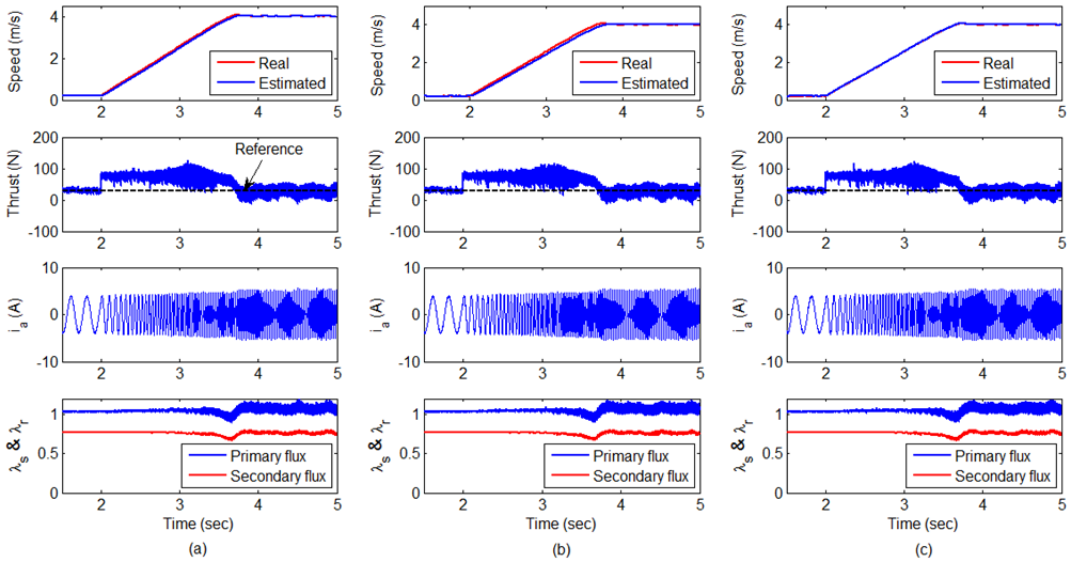

Fig. 8. Linear speed, thrust, phase-A current, primary and secondary flux for low to rated speed maneuver using (a) PI controller (b) Fuzzy controller (c) Mechanical model (simulation).

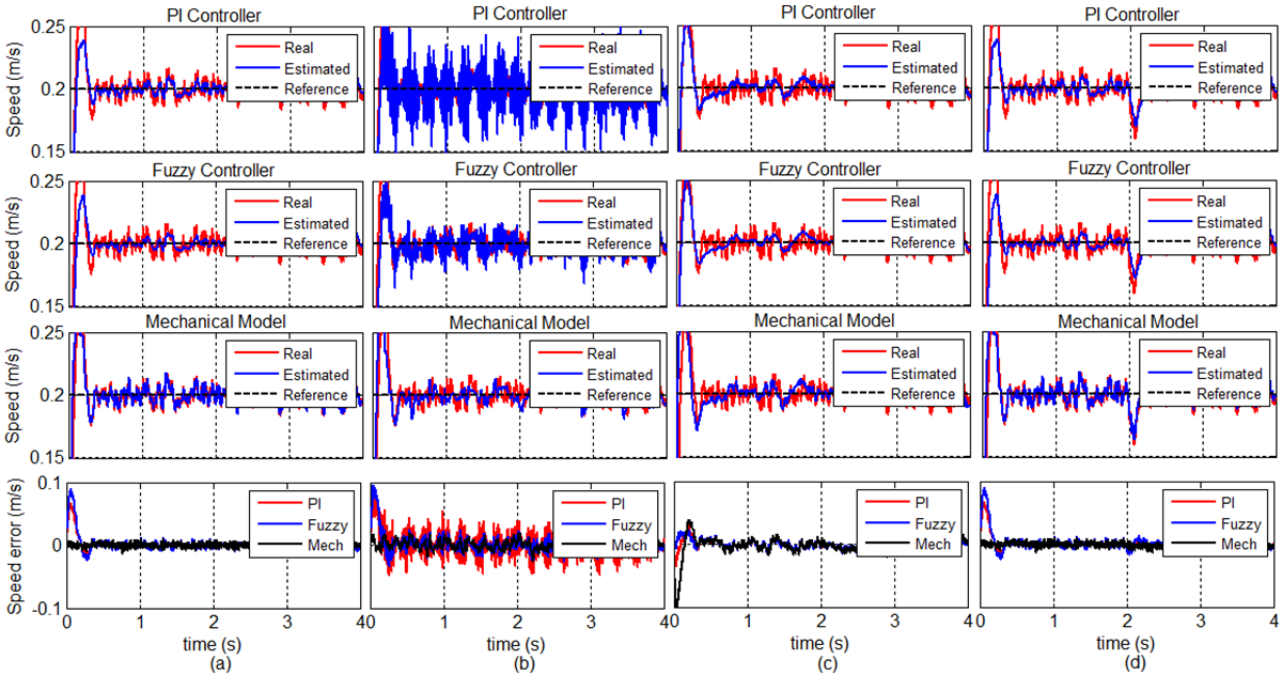

Fig. 9. The operation of MRAS based speed estimator for (a) normal condition (b) noisy condition (c) machine parameter variation (d) load force change (simulation).

speed properly follows the real speed for all adaptation mechanisms, however, the mechanical model has better performance against fuzzy and PI controller especially in the transient region. Moreover, despite the step change in linear speed, thrust and secondary flux of LIM still follow its command values.

B. Low Speed Operation

The main focus of this study is the operation of MRAS speed estimator at a very low speed because the range of speed is the most critical case for estimators. The speed command chosen, $0.2\,m/s$, is 5% its nominal value.

In order to evaluate the adaptation mechanisms, two indices, based on speed error, are introduced as follows:

$$Index1 = 1000 \times \int_0^{t_d} t\left|\Delta v_l\right| dt \tag{28}$$

$$Index2 = 1000 \times \int_{td}^{t_{sim}} t\left|\Delta v_l\right| dt \tag{29}$$

where t_d is the acceleration time of motor with a value of 0.5s. The first index indicates the transient behavior of MRAS speed estimator, whereas the second one considers the

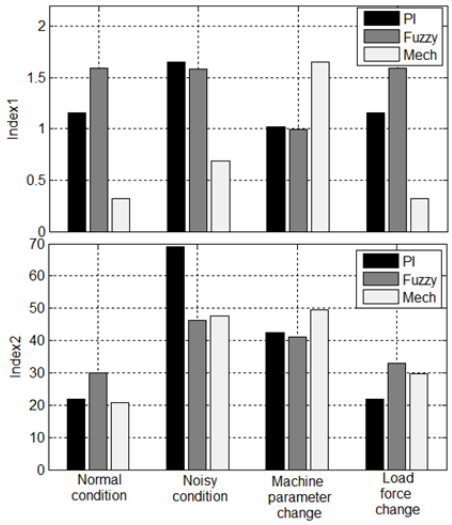

Fig. 10. The values of indices.

TABLE II
THE OVERALL INDEX

Adaptation mechanisms	Normal condition	Noisy condition	Machine parameter change	Load force change
PI Controller	23.039	70.691	43.435	25.087
Fuzzy controller	31.66	47.713	42.112	34.66
Mechanical model	21.145	48.346	51.234	30.022

steady-state operation. Robustness of the MRAS speed estimator with the conventional/proposed adaptation mechanisms for LIM is verified at four different modes:

1) Normal condition
2) Noisy condition: A white noise is applied in measured voltage and current signals. These signals are used as input of the secondary flux estimators (voltage and current model). This type of noise can be caused by thermal changes and their impact on electronic carrier.
3) Machine parameter variation: The secondary resistance of LIM is increased by 20% compared with normal condition.
4) Load force change: The load force disturbance is lightly increased as a step function, from $0\,N$ to $30\,N$ at $t = 2\,s$.

The operation of MRAS speed estimator with PI, fuzzy, and mechanical adaptation mechanisms in normal condition, is shown in Fig. 9(a). From this figure, the mechanical adaptation mechanism properly estimates linear speed at transient and steady-state operation. Index1 value is 0.322, 1.154, and 1.594 for mechanical adaptation mechanism, PI, and fuzzy controller, respectively. One of the significant advantages of mechanical adaptation mechanism is the improvement of transient operation of the estimator.

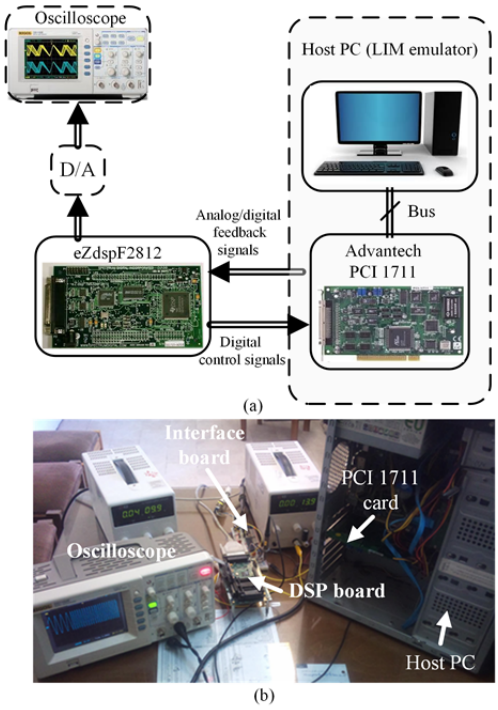

Fig. 11. Real-time HIL structure (a) schematic diagram (b) experimental layout.

The behavior of the speed estimator with PI, fuzzy and mechanical adaptation mechanisms for noisy condition is shown in Fig. 9(b). The PI controller is significantly affected by measurement noise, whereas fuzzy and mechanical adaptation mechanisms are more robust against noise. In this case, Index2 is 69.042, 46.129 and 47.661 for PI, fuzzy and mechanical adaptation mechanisms, respectively.

The real and estimated speed of LIM for PI, fuzzy, and mechanical adaptation mechanisms, as well as the speed error, when the secondary resistance has 20% variations, is shown in Fig. 9(c). The machine parameter variations caused the operation of all adaptation mechanisms to deteriorate, but the mechanical model is more effective. In this case, Index2 is 42.414, 41.12 and 49.586 for PI, fuzzy, and mechanical adaptation mechanism, respectively. Furthermore, the variation rate of Index2, in contrast to normal condition, is 58%, 26.88% and 48.4% for PI, fuzzy and mechanical adaptation mechanisms, respectively; the values show thatfuzzy controller has a stable behavior against machine parameter variations.

The operation of MRAS speed estimator, when the load force disturbance is applied to LIM, is shown in Fig. 9 (d). A summary of results about the MRAS speed estimator operation based on PI, fuzzy and mechanical adaptation mechanisms at four aforementioned described modes, from the viewpoint of transient and steady-state behavior of LIM (Index1 and Index2) are shown in Fig. 10. In most applications, both transient and steady-state operations of the drive system have significant roles in the definition of an

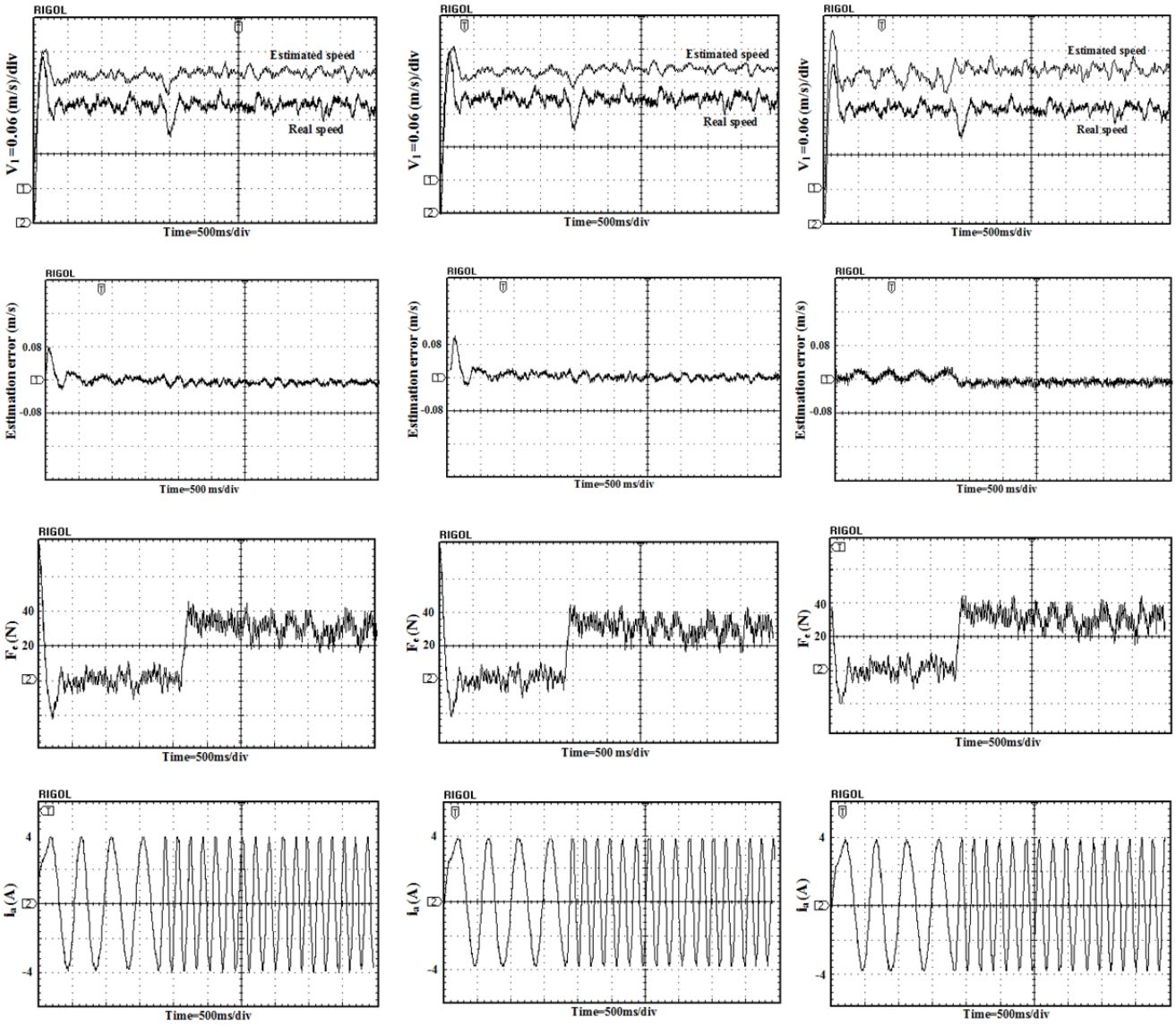

(a) (b) (c)

Fig. 12. The estimated linear speed, estimation error of speed, thrust and phase-a current for load force change by (a) PI (b) fuzzy (c) mechanical adaptation mechanisms (Real-time HIL simulation).

objective function. In general, the objective function can be obtained from a weighted combination of two mentioned indices. In this study, according to equation (27), both indices have the same weight in objective function. Therefore, the overall index, which is defined as the sum of Index1 and Index2, is shown in Table II.

IX. Real-Time Hardware-in-the-Loop Simulation

Real-time hardware-in-the-loop (HIL) simulation is an effective and emerging strategy for advanced testing which provides a connection between simulation and real condition. In essence, from the viewpoint of accuracy of real condition simulation, real-time HIL method is located between experimental testing and conventional software-based simulation. This approach is widely used in automotive and aerospace industries, high-scale power electronic converters, and electric machine drive studies, where a piece of system is not available or the real system test is devastating [21], [22].

In an HIL simulation, if the physical hardware of studied system is not available for experimentation, it can be replaced by an emulated hardware in the testing loop. Because of the existence of these parts of real system in the control loops and considering the real-time behavior of controller, the HIL approach increases the authenticity of the simulation. The running time of emulated parts must not be more or less than

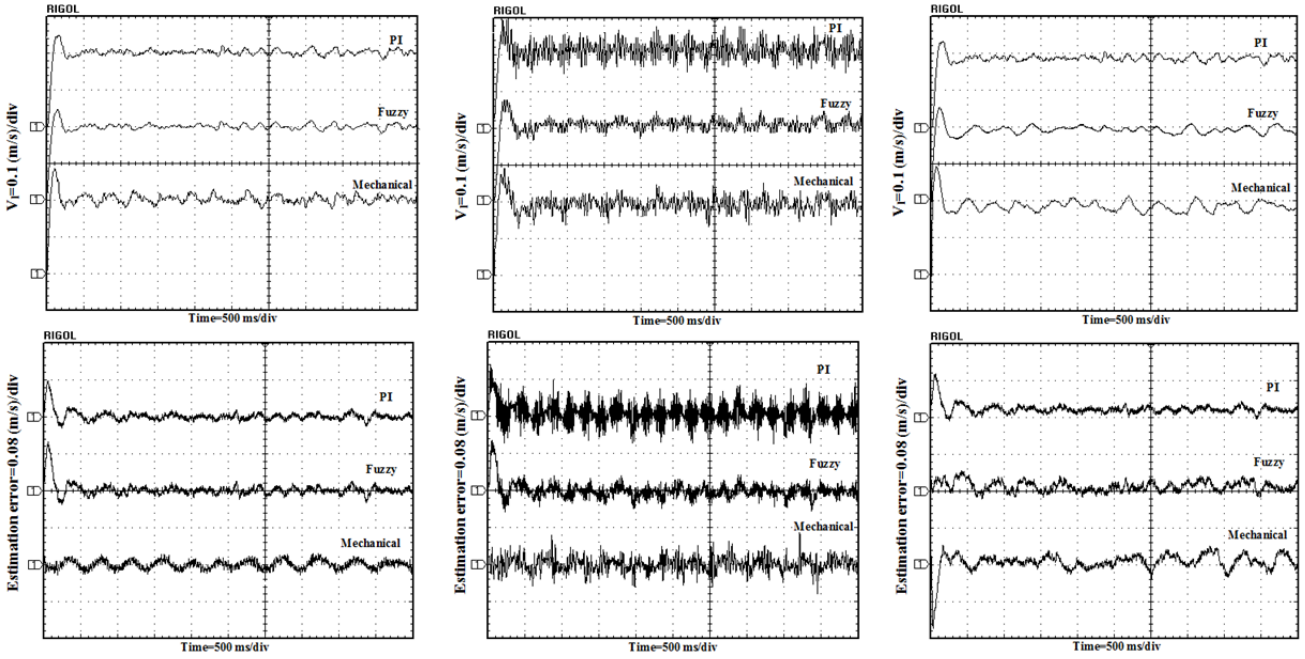

(a) (b) (c)

Fig. 13. The estimated linear speed and estimation error of speed by PI, fuzzy and mechanical adaptation mechanisms in (a) normal condition (b) noisy condition (c) machine parameter change (Real-time HIL simulation).

real-time. In order to obtain a real-time based HIL simulation, the Matlab/Real-time windows target toolbox is adopted and the performance of MRAS speed estimator with the proposed adaptation mechanisms is clarified by this approach.

The schematic diagram and experimental layout of real-time HIL method are shown in Figs. 11 (a) and (b), respectively. In the HIL method, the vector control scheme with MRAS speed estimator is implemented on an ezdspF2812 board. The LIM dynamic model and nonlinear model of inverter, described in [23], is simulated on a host personal computer (PC). In this scheme, the host PC is used as LIM and as an inverter emulator. The real-time control commands of DSP board are applied to the host PC as digital control signals by using an Advantech PCI 1711 card which is located on a PC bus. The analog/digital feedback signals are returned to DSP board and subsequently processed to obtain next control commands. Moreover, an interface board is used to send data from DSP board to oscilloscope. In the experimental testing, the host PC (LIM emulator) is replaced by LIM and inverter board. Therefore, the real-time property of experimental testing remains in the HIL method.

The estimated linear speed, estimation error of speed, thrust, and phase-a current by PI, fuzzy, and mechanical adaptation mechanisms at low speed from real-time HIL method are shown in Fig. 12. The linear speed command is $0.2\,m/s$ and the load force disturbance is applied to LIM at $t = 2s$ as a step function from $0\,N$ to $30\,N$. From this figure, it is clear that the estimated linear speed and thrust properly track its command values. The estimation error of speed shows that mechanical model based adaptation mechanism improves the transient behavior of speed estimator for this operation condition. Despite the high overshoot of estimated speed from mechanical adaptation mechanism, the performance in acceleration time of motor is better because the transient estimation error of speed is lower. Based on the fact that mechanical adaptation mechanism is directly designed from a mechanical equation of LIM and some mechanical parameters, such as moving mass, the mechanism has a great effect on transient behavior of motor. Also, fuzzy and PI adaptation mechanisms are roughly similar especially from the Index1 standpoint. Hence, results obtained from the real-time HIL method confirm the simulation results. In a low speed operation, applying the rated load force to LIM is not allowed because the motor may be stopped under this force. Therefore, a light load force (30 N) is applied to LIM whereby the amplitude of phase current is slightly and intangibly changed but the frequency of phase current is increased to maintain linear speed at its reference value.

The estimated linear speed and its estimation error in normal condition, noisy condition and machine parameter change by PI, fuzzy, and mechanical adaptation mechanisms are shown in Figs. 13(a) , (b) and (c), respectively. Both fuzzy controller and mechanical model effectively improve the operation of MRAS speed estimator in a noisy condition, where the mechanical model has better transient performance. On the other hand, the fuzzy controller has better transient and steady-state behavior when secondary resistance of LIM

is changed by 20%. Also, by comparing the operations of fuzzy controller under different conditions, the robustness of the method is observed because the estimation error of the fuzzy controller is more stable under normal conditions than under any other undesirable conditions.

X. CONCLUSION

This paper proposes two novel adaptation mechanisms, instead of a conventional fixed-gain PI controller, to improve the operation of LIM, particularly at very low speeds. The first scheme utilizes fuzzy controller, and the second one is derived from a mechanical equation of LIM. In the preliminary step using the proper dynamic model of LIM, the flux estimators based on voltage and current models are deduced. Afterward, the estimators are combined to constitute MRAS based speed estimator where both models estimate the secondary flux in a stationary reference frame. The adaptation mechanism provides linear speed using the speed tuning signal. The optimum parameters of adaptation mechanisms (PI controller, fuzzy controller, and mechanical model) are obtained by COA. In order to validate the operation of the proposed schemes, a comparative study is presented with the following four different modes: normal condition, noisy condition, machine parameter variation, and load force change. Both simulation and real-time HIL results show that the proposed schemes improve the operation of MRAS speed estimator at noisy condition and machine parameter variations. In this regard, the mechanical model strongly enhances the transient behavior of a speed estimator. The fuzzy controller is more robust against a variation of machine parameters. Furthermore, both fuzzy controller and mechanical model improve the operation of speed estimator against voltage and current measurement noises.

APPENDIX

TABLE III
THE STUDY SYSTEM PARAMETERS

SLIM parameters		**Optimum parameters of adaptation mechanisms by COA**		
p	6	**PI controller**		
$L_{ls}[mH]$	69	$K_p = 5.5$	$K_i = 137.5$	
$L_{lr}[mH]$	0	**Fuzzy controller**		
$L_m[mH]$	200	$K_1 = 0.0191$	$K_2 = 5.98$	$K_3 = 0.23$
$R_s[\Omega]$	10.6	**Mechanical model**		
$R_r[\Omega]$	32	$K_{pv} = 1000$	$K_{pf} = -500$	
$M[Kg]$	20			

REFERENCES

[1] T. A. Nondahl and D. W. Novotny, "Three-phase pole-by-pole model of a linear induction machine," in *Proc. IEE.*, Vol. 127, No. 2, pp. 68-82, Mar. 1980.

[2] W. Xu, G. Sun, G. Wen, Z. Wu, and P. K. Chu, "Equivalent circuit derivation and performance analysis of a single-sided LIM based on the winding function theory," *IEEE Trans. Veh. Techol.*, Vol. 61, No. 4, pp. 1515-1525, May 2012.

[3] R. M. Pai, I. Boldea, and S. A. Nasar, "A complete equivalent circuit of an LIM with sheet secondary," *IEEE Trans. Magn.*, Vol. 24, No. 1, pp. 639-654, Jan 1988.

[4] J. F. Gieras , G. E. Dawson, and A. R. Easthan, "A new longitudinal end effect factor for linear induction motors," *IEEE Trans. Energy Convers.*, Vol. 2, No. 1, pp. 152-159, Mar. 1987.

[5] W. Xu, J. G. Zhu, Y. Zhang, Z. Li, Y. Li, Y. Wang, Y. Guo, and W. Li, "Equivalent circuits for single-sided linear induction motors," *IEEE Trans. Ind. Appl.*, Vol. 46, No. 6, pp. 2410-2423, Nov./Dec. 2010.

[6] J. Faiz and H. Jafari, "Accurate modeling of single-sided LIM considers end effect and equivalent thickness," *IEEE Trans. Magn.*, Vol. 36, No. 5, pp. 3785-3790, Sep. 2000.

[7] C. Huang and L. Fu, "Adaptive approach to motion controller of linear induction motor with friction compensation," *IEEE/ASME Trans. Mechatron.*, Vol. 12, No. 4, pp. 480-490, Aug. 2007.

[8] J. Duncan, "Linear induction motor-equivalent-circuit model," *IEE Proc. Electr. Power Appl.*, Vol. 130, No. 1, pp. 51-57, Jan. 1983.

[9] J. H. Sung and N. Kwanghee, "A new approach to vector control for a linear induction motor considering end effects," *Industry Applications Conference, 1999. Thirty-Fourth IAS Annual Meeting. Conference Record of the 1999 IEEE*, Vol. 4, pp. 2284-2289, Sep. 1999.

[10] G. Kang, K. Nam, "Field-oriented control scheme for linear induction motor with the end effect," *IEE Proc. Electr. Power Appl.*, Vol. 152, No. 6, pp. 1565-1572, Nov. 2005.

[11] M. Pucci, "Direct field oriented control of linear induction motors," *Electr. Power Syst. Res.*, Vol. 89, pp. 11-22, Aug. 2012.

[12] M. Cirrincione, A. Accetta, M. Pucci, and G. Vitale, "MRAS speed observer for high performance linear induction motor drives based on linear neural networks," *IEEE Trans. Power. Electron.*, Vol. 28, No. 1, pp. 123-134, Jan. 2013.

[13] P. Liu, C. Y. Hung, C. S. Chiu, and K. Y. Lian, "Sensorless linear induction motor speed tracking using fuzzy observers," *IET Elect. Power Appl.*, Vol. 5, No. 4, pp. 325-334, Apr. 2011.

[14] S. M. Gadoue, D. Giaouris, and J. W. Finch, "MRAS sensorless vector control of an induction motor using new sliding-mode and fuzzy-logic adaptation mechanisms," *IEEE Trans. Energy Convers.*, Vol. 25, No. 2, pp. 394-402, Jun. 2010.

[15] P. Vas, *Sensorless Vector and Direct Torque Control*, New York: Oxford Univ. Press, 1998.

[16] C. Schauder, "Adaptive speed identification for vector control of induction motors without rotational transducers," *IEEE Trans. Ind. Appl.*, Vol. 28, No. 5, pp. 1054-1061, Sep./Oct. 1992.

[17] S. Mir, M. E. Elbuluk, and D. S. Zinger, "PI and fuzzy estimators for tuning the stator resistance in direct torque

control of induction machines," *IEEE Trans. Power. Electron*., Vol. 13, No. 2, pp. 279-287, Mar. 1998.
[18] J. Maes and J. Melkebeek, "Speed-sensorless direct torque control of induction motors using an adaptive flux observer," *IEEE Trans. Ind. Appl*., Vol. 36, No. 3, pp. 778-785, May/Jun. 2000.
[19] H. Shayeghi, H. A. Shayanfar, S. Jalilzadeh, and A. Safari, "Multi-machine power system stabilizers design using chaotic optimization algorithm," *Energ Convers Manage*, Vol. 51, No. 7, pp. 1572-1580, Jul. 2010.
[20] D. Yang, G. Li, and G. Cheng, "On the efficiency of chaos optimization algorithms for global optimization," *Chaos Soliton Fract*, Vol. 34, No. 4, pp. 1366-1375, Nov. 2007.
[21] J. H. Jung, "Real-time and power hardware-in-the-loop simulation of PEM fuel cell stack system," *Journal of Power Electronics*, Vol. 11, No. 2, pp. 202-210, Mar. 2011.
[22] C. S. Edrington, O. Vodyakho, and B. A. Hacker, "Development of a unified research platform for plug-in hybrid electrical vehicle integration analysis utilizing the power hardware-in-the-loop concept," *Journal of Power Electronics*, Vol. 11, No. 4, pp. 471-478, Jul. 2011.
[23] J. Holtz, "Pulsewidth modulation for electronic power conversion," *IEEE Proc*., Vol. 82, No. 8, pp. 1194-1214, Aug. 1994.

Mohammad Hosein Holakooie was born in Tehran, Iran. He received his B.Sc. and M.Sc. degrees in electrical engineering from Guilan and Tabriz University, respectively. He is currently working toward a Ph.D. degree in electrical engineering at Zanjan university. His current research interests include analysis and control of rotary and linear electric machines, power electronic converters, and electrical machine design.

Asghar Taheri was born in Zanjan, Iran, in 1977. He received his B.S., M.S., and Ph.D. degrees, all in electronics engineering, from the Amirkabir University of Technology and the Iran University of Science and Technology, Tehran, Iran, in 1999, 2001, and 2011, respectively. He has been a member of the faculty at the University of Zanjan since 2010 where he is currently an Assistant Professor. His current research interests include motor drives and control, and multi phase machine drives, power electronic systems design, process control, DSP and FPGA based system designs, hardware in the loop, and computer-aided control.

Mohammad Bagher Bannae Sharifian was born in Tabriz, Iran, in 1965. He received his B.S. and M.S. degrees in Electrical Engineering from the Department of Engineering, University of Tabriz, Tabriz, Iran, in 1989 and 1992, respectively. In 1992, he joined the Faculty of Electrical and Computer Engineering, University of Tabriz. He received his Ph.D. degree in Electrical Engineering from the Department of Electrical and Computer Engineering, University of Tabriz, in 2000. He was an Assistant Professor from 2000 to 2004, an Associate Professor from 2004 to 2009 and has been a Professor since 2009. His research interests include design, modeling, and analysis of electrical machines, transformers, liner electric motors, and electric and hybrid electric vehicle drives.